



Ozone deposition measurements over wheat fields in the North China Plain: variability and related factors of deposition flux and velocity

5 Xiaoyi Zhang^{1,2}, Wanyun Xu^{1,*}, Weili Lin³, Gen Zhang¹, Jinjian Geng^{4,5}, Li Zhou^{4,5}, Huarong Zhao^{4,5},
Sanxue Ren^{4,5}, Guangsheng Zhou^{4,5}, Jianmin Chen² and Xiaobin Xu^{1,*}

¹ State Key Laboratory of Severe Weather, Key Laboratory for Atmospheric Chemistry, Institute of Atmospheric Composition, Chinese Academy of Meteorological Sciences, Beijing, China, 100081

² Department of Atmospheric and Oceanic Sciences, Fudan University, Shanghai, China, 200433

³ College of Life and Environmental Sciences, Minzu University of China, Beijing, China, 100081

10 ⁴ State Key Laboratory of Severe Weather, Institute of Agricultural Meteorology, Chinese Academy of Meteorological Sciences, Beijing, China, 100081

⁵ Hebei Gucheng Agricultural Meteorology National Observation and Research Station, Baoding, China, 072656

Correspondence to: Wanyun Xu (xuwy@cma.gov.cn) and Xiaobin Xu (xiaobin_xu@189.cn)

Abstract. Ozone (O₃) deposition is closely related to air quality, ecosystem and climate changes. Due to the instrument and
15 method shortage, O₃ deposition was less observed and investigated in China, experiencing significantly increasing O₃
exposure. Here, we conducted a comprehensive measurement of O₃ deposition over the wheat canopy at a typical polluted
agricultural site in the North China Plain using a newly developed relaxed eddy accumulation system. For the main wheat
growing season in 2023, O₃ deposition flux and velocity (V_d) averaged $-0.25 \pm 0.39 \mu\text{g m}^{-2} \text{ s}^{-1}$ and $0.29 \pm 0.33 \text{ cm s}^{-1}$,
respectively. Daytime V_d ($0.40 \pm 0.38 \text{ cm s}^{-1}$) was obviously higher than in the nighttime ($0.17 \pm 0.26 \text{ cm s}^{-1}$). The temporal
20 changes of V_d were mainly determined by crop growth, with predominant contribution of stomatal uptake. Both daytime and
nighttime V_d exhibited significant increases with decreasing relative humidity, and increasing friction velocity and soil water
content, enhanced by higher leaf area index. With rapid increases of soil moisture, simultaneous and following overall
increments in V_d were detected, attributed to remarkably strengthening O₃ stomatal uptake under increased stomatal
conductance and extended opening to the night, and more non-stomatal O₃ removal at night resulted from strengthened soil
25 NO emission at moist conditions. This study confirms the leading effects of crop growth on O₃ deposition modulated by
environmental conditions and the non-negligible influences of nocturnal plant activities, and emphasizes the needs for O₃
deposition observation over different surfaces and accurate evaluation of O₃ agricultural impacts based on deposition fluxes.

1 Introduction

30 Surface ozone (O₃) is a key secondary air pollutant, generated in photochemical reactions involving volatile organic
compounds (VOCs), nitrogen oxides (NO_x = NO + NO₂), etc. (Seinfeld et al., 2006). Over the past two decades, China's
rapid economic development and increasing anthropogenic emissions of NO_x and VOCs have led to significantly upward



trends in O₃ concentrations (Monks et al., 2015; Li et al., 2019; Lu et al., 2020; Xu et al., 2020), especially in the North China Plain (NCP) (Tai et al., 2014; Ma et al., 2016; Wang et al., 2017; Lu et al., 2020; Xu, 2021; Wang et al., 2022; Lyu et al., 2023). Dry deposition plays one of the key roles in removing surface O₃ (e.g., Tang et al., 2017) and in the budget of tropospheric O₃ (Lelieveld and Dentener, 2000). Over vegetated areas, stomatal and non-stomatal uptake of O₃ may represent major part of the total dry deposition (Fowler et al., 2001). Uptake of higher amount of O₃ may cause a series of hazardous oxidative reactions, damaging vegetation and threatening crop quality and production (Ainsworth, 2017; Harmens et al., 2018; Mills et al., 2018; Feng et al., 2019b). In addition, O₃ deposition to the ground surfaces (including soil, snow and water) is closely related to tropospheric chemistry, air quality and ecosystems (Clifton et al., 2020a; Stella et al., 2019; Helmig et al., 2012; Stocker et al., 1995). It is estimated that O₃ dry deposition contributes about 20% to the annual global tropospheric O₃ loss (Lelieveld and Dentener, 2000; Wild, 2007; Hardacre et al., 2015). Under the rapid expansion of population and growing demands for food, China has become the largest crop producer, as well as importer (Dong et al., 2021). O₃ deposition is thus of great importance and its accurate quantification is urgently needed to evaluate the impact of increasing O₃ levels on agricultural production, ecological environment, air quality, human health, and global climate.

O₃ deposition has been measured over various ecosystems, including forest, grassland, cropland and bare soil environments (Table S1), in order to understand deposition mechanisms and evaluate its potential effects (Stella et al., 2019; Xu et al., 2018; Zhu et al., 2015; Helmig et al., 2012; Mészáros et al., 2009; Lamaud et al., 2009; Coyle et al., 2009). However, the deposition processes are controlled by various biotic (stomatal uptake) and abiotic (non-stomatal removal) activities that are simultaneously modulated by the environmental factors. The relative contributions of stomatal and non-stomatal O₃ deposition varied with land cover, plant species and growth stages, as well as environmental factors. Stomatal uptake of O₃ depends on the opening and closure of stomata on leaf surfaces. For example, the fraction of diurnal maximum stomatal O₃ deposition over boreal forests ranged from 56 to 74% (Rannik et al., 2012), while only accounting for 31.2% in a wheat field (Xu et al., 2018). Non-stomatal resistance of O₃ decreased with the increasing temperature and friction velocity, and was ~ 50% lower under wet conditions than under dry conditions over the same potato canopy (Coyle et al., 2009). Thus, O₃ deposition is dominated by distinct deposition processes over different surfaces in different environments.

Currently, the eddy covariance (EC) method is the most commonly used micrometeorological technique for measuring vertical fluxes and is also regarded as the most ideal method (Businger, 1986; Baldocchi et al., 1988). However, it requires robust fast-response measurement instruments (≥ 10 Hz), which limits the flux measurements of various reactive gases due to the lack of high frequency detection techniques (Hicks and Wesely, 1978; Muller et al., 2009). The flux-gradient (FG) approach is the most important alternative method for O₃ flux measurements (Stella et al., 2012; Loubet et al., 2013; Wu et al., 2015), which is based on the flux-gradient relationship (K-theory) (Baldocchi, 1988). The assumption of flux-gradient relationship is dependent on surface roughness and the photochemical reactions of O₃ and its precursors, which does not hold over rough heterogeneous surfaces (such as forests) and when O₃ formation reaction rates exceed turbulent mixing rates (Raupach and Thom, 1981; Vilà-Guerau De Arellano and Duynkerke, 1992). Besides, FG needs simultaneous O₃ concentration measurements at several heights (2 ~ 4) and accordingly requires several parallel O₃ analyzers (Loubet et al.,



2013). These relatively high requirements of instruments have more or less limited the application of traditional micrometeorological methods to the measurements of O₃ flux.

The relaxed eddy accumulation (REA) method is an alternative method for observing the air-surface exchange of interested substances over ecosystems, which is based on the same physical principle as EC (Desjardins, 1977; Businger and Oncley, 1990; Pattey et al., 1993). The fluxes in REA systems are obtained by accumulating and accurately measuring the air associated with updrafts and downdrafts at a constant flow rate in two separate reservoirs (Businger and Oncley, 1990). REA methods have been widely applied in flux measurements of various species, such as biogenic VOCs (Mochizuki et al., 2014; Moravek et al., 2014), peroxyacetyl nitrate (Moravek et al., 2014), reduced sulfur gases (Xu et al., 2002), HONO (Ren et al., 2011), aerosols (Matsuda et al., 2015; Xu et al., 2021), NH₃ and Hg (Osterwalder et al., 2016). To the best of our knowledge, the REA method has not been applied in O₃ deposition flux measurements so far.

Although many regions in China have been experiencing severe O₃ pollution during growing seasons, measurements of O₃ flux over crop fields in the country have only sporadically reported, which were made using either chamber techniques (e.g., Tong et al., 2015) or micrometeorological approaches (Zhu et al., 2014; Zhu et al., 2015; Xu et al., 2018). In this study, we developed a new REA flux system and applied it to obtain O₃ deposition fluxes over wheat fields in the NCP during the springtime growing season. Based on these in-situ observations, we evaluated the feasibility of O₃ flux measurements using the REA method, analyzed the variation characteristics of O₃ deposition during the wheat growing season, identified the key drivers in the variability of daytime and nighttime O₃ deposition during distinct crop growth stages and different environmental conditions, respectively.

2 Observation and method

2.1 Site description

The flux observations were conducted at the Gucheng site (39°08'N, 115°40'E, GC), an integrated ecological-meteorological observation and research station of the Chinese Academy of Meteorological Science, located 35 km to the northeast of urban Baoding City, Hebei Province, and 100 km southwest to urban Beijing. The site is surrounded mainly by flat, irrigated high-yield agricultural lands in the northern part of the NCP (see Fig. 1a in Zhang et al., 2022b). The fields within and surrounding the yard of GC are on a winter wheat-summer maize rotation, which is typical in Northern China. Observations at the site have revealed good regional representativeness of the polluted agricultural areas in the NCP (Lin et al., 2009; Xu et al., 2019; Kuang et al., 2020; Zhang et al., 2022a).



2.2 Relaxed eddy accumulation (REA) technique

2.2.1 Theory

95 A homemade relaxed eddy accumulation system for O₃ dry deposition measurements (REA-O₃ flux system) was deployed at GC. In the REA-O₃ flux system, conditional sampling is conducted according to the direction of vertical wind (w), which separates sampled air into updraft and downdraft reservoirs at a constant flow rate. The vertical fluxes of O₃ (F_{O_3} , in $\mu\text{g m}^{-2} \text{s}^{-1}$) are calculated by the concentration differences between two reservoirs following Eq. (1):

$$F_{O_3} = \overline{w' c'} = b \sigma_w (\overline{c^+} - \overline{c^-}), \quad \text{Eq. (1)}$$

100 where σ_w is the standard deviation of vertical wind (in m s^{-1}); $\overline{c^+}$ and $\overline{c^-}$ are the averaged O₃ concentrations in the updraft and downdraft reservoirs, respectively (in $\mu\text{g m}^{-3}$); b is the eddy accumulation coefficient and is obtained from CO₂ flux measured using the EC method and calculated using Eq. (2):

$$b = \frac{\overline{w' CO_2'}}{\sigma_w (\overline{CO_2^+} - \overline{CO_2^-})}, \quad \text{Eq. (2)}$$

105 where $\overline{CO_2^+}$ and $\overline{CO_2^-}$ are averaged CO₂ concentration observed under upward and downward vertical winds, respectively (in mg m^{-3}), $\overline{w' CO_2'}$ represents the EC CO₂ flux (in $\text{mg m}^{-2} \text{s}^{-1}$). Based on the measurements from February to June, b revealed an average \pm standard deviation of 0.55 ± 0.09 , ranging from 0.16 to 0.80.

O₃ deposition velocity (V_d , cm s^{-1}) is estimated based on O₃ flux and concentrations using Eq. (3):

$$V_d = -\frac{F_{O_3}}{C_{O_3}} \times 100, \quad \text{Eq. (3)}$$

where C_{O_3} is the 30 min averaged O₃ concentration (in $\mu\text{g m}^{-3}$).

110 2.2.2 System setup and verification

The setup of the REA-O₃ flux system is depicted in Figure 1. A 3-D sonic anemometer (CSAT3, Campbell Scientific Inc., USA) was used for measuring the three wind components (u , v , w) at 10 Hz, which was amounted at the height of 4.5 m on an eddy covariance tower. The inlet (1/8" OD Teflon tubing) of the REA system was installed in the center of the anemometer. The 10 Hz wind signals, together with the signals from the CO₂/H₂O analyzer (Li-7500, LI-COR, Inc., USA),
115 were collected by a datalogger (CR1000, Campbell Scientific Inc., USA) and sent to a PC. The wind signals were processed by a program written in Python, which also sent switch command to two fast-response 3-way solenoid valves based on the vertical wind direction. Sample air was thus pumped alternatively into sample tubes (1/4" OD Teflon) for updraft or downdraft based on the direction of instantaneous vertical winds and analyzed by two UV photometric O₃ analyzers (TE 49i, Thermo Fisher Scientific Inc., USA) installed at the ends of updraft and downdraft channels, respectively. To ensure the
120 stability of airflow in the O₃ analyzers and sampling system, zero air was supplied to the channel that was not sampling ambient air. In addition, both sampling tubes were bypassed to increase the inlet sample flow and avoid the axial mixing before the solenoid valves. The linear velocity of air sample in the inlet tubing was set to 22 m s^{-1} , and airflow was at the



turbulent state with a Reynolds number over 2300. The estimated residence time from system inlet to the valves was 18 ms and the REA system was working at a sample frequency of 10 Hz. The O₃ analyzers recorded 1-minute averaged O₃ concentrations, which were downloaded by the PC. The actual averaged O₃ concentrations under updraft and downdraft conditions were calculated according to Eq. (4) using the sample time, sample flow and 1-minute averaged O₃ concentrations:

$$\bar{c} = \frac{\sum_{i=1}^{30} c_i \times flow_i}{\sum_{i=1}^{30} flow_i \times t_{sample\ gas,i}}, \quad \text{Eq. (4)}$$

where c_i is the 1-minute averaged O₃ concentration (in $\mu\text{g m}^{-3}$), $flow_i$ is the 1-minute averaged sample flow (in SLPM) measured by the mass flow meter (MFM), and $t_{sample\ gas,i}$ the real time for analyzing air sample within i th minute (in fraction of a minute).

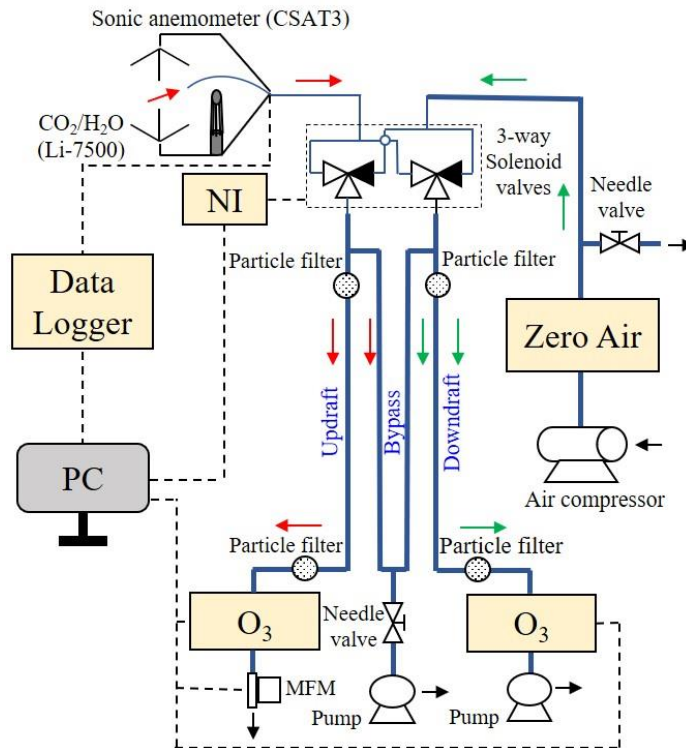


Figure 1: Schematic of the REA-O₃ flux system ($w > w_0$).

To increase the concentration difference between updraft and downdraft, a wind speed threshold called the wind dead-band (w_0) was used in the REA system to discard air samples associated with w close to 0. The application of w_0 promotes the sampling of larger eddies that contribute more to gas fluxes. If a proper w_0 is used, the eddy frequency spectrum shifts to the low frequencies in the sample, but does not cut off all the high-frequency signals, only filtering out samples with small vertical displacements that have relatively small impacts on the overall flux (Bowling et al., 1999; Held et al., 2008; Tsai et al., 2012; Moravek et al., 2014; Grelle and Keck, 2021). Conditional sampling using w_0 also prolongs the lifetime of the fast-



response solenoid valves (Pattey et al., 1993) and effectively avoids sampling error around $w = 0$ due to the limitation of the
140 sonic anemometer (Grelle and Keck, 2021). In the REA-O₃ system, we adopted fixed wind dead-bands during the daytime
(from 08:00 to 18:00 Local Time (LT), $w_0 = 0.05 \text{ m s}^{-1}$) and night (from 19:00 to 07:00 LT, $w_0 = 0.01 \text{ m s}^{-1}$), respectively,
considering that wind speeds during the daytime were generally larger than those at night. The concentration difference
increased with w_0 and led to an increase in measured fluxes. Figure S1 shows the comparison of REA CO₂, H₂O and heat
145 fluxes under conditional sampling adopting w_0 and full sampling, respectively, calculated using raw EC data with a constant
 b of 0.60 (Businger and Oncley, 1990). The two flux datasets revealed excellent correlations, with a correlation coefficient
close to 1, proving the reliability and stability of the REA flux measurement system. Compared with the fluxes without w_0 ,
CO₂, H₂O and heat fluxes with w_0 exhibited similar small overestimations, reaching around 10-13% during the daytime and
4-10% at night, which were comparable with the influence of a dynamic dead-band ($w_0 = \frac{\sigma_w}{0.35}$) in Grelle and Keck's (2021)
150 REA system for H₂O, CO₂, CH₄, N₂O flux measurements. This indicates that adopting the wind dead-band in our REA
system only had marginal impact on observed fluxes.

To identify potential flux errors induced by any differences between updraft and downdraft channels in the REA-O₃
system (including valves, sample tubes and O₃ analyzers), we checked the parallel of sampling system by simultaneous
measurements of ambient O₃ from the inlet. As shown in Figure S2, O₃ data points obtained from the two channels all
aligned close to the 1:1 line (slope = 1.02), suggesting that the difference in measured O₃ was minimal between updraft and
155 downdraft and its impact on flux measurement can be ignored. Moreover, synchronous multipoint calibrations of the two
channels were conducted monthly. Different O₃ concentrations generated by an O₃ calibrator (TE 49C PS, Thermo Fisher
Scientific Inc., USA) were introduced into the system from the zero air inlet and simultaneously measured by the two O₃
analyzers.

To further verify the reliability of the REA system, we also compared the fluxes data derived from the REA technique
160 with w_0 and EC theory. For CO₂, H₂O and heat, the averaged ratios of REA to EC fluxes were all slightly larger than 1,
indicating small overestimates in the REA flux measurement system, which were expected due to the use of w_0 . Most of the
flux data maintained high consistency with correlation coefficients close to 1 (Figure S3), confirming that the REA system
performed reliably under most conditions.

2.3 Field measurements and ancillary data

165 Measurements of O₃ flux were conducted during the main wheat growing season in 2023, from the late of dormancy stage
(13 February 2023) to wheat harvest (18 June 2023). Ancillary data were obtained for further analysis. Meteorological
variables including air temperature (T_{Air}), relative humidity (RH), precipitation, soil temperature (T_{Soil}) and volumetric water
content (soil VWC) at 20 cm, global solar radiation (G), photosynthetic active radiation (PAR) and sun elevation angle were
measured by an automatic weather station at GC. The 30 min CO₂, H₂O, heat and momentum fluxes were measured by the
170 EC system, which includes a 3-D sonic anemometer, an open path CO₂/H₂O analyzer and a datalogger. The friction velocity



(u_*) was calculated using the three wind components (u , v , w) following Eq. (5), and the vapor pressure deficit (VPD) was estimated as in Eq. (6).

$$u_* = \left(\overline{u'w'}^2 + \overline{v'w'}^2 \right)^{1/4}, \quad \text{Eq. (5)}$$

$$VPD = \left(1 - \frac{RH}{100} \right) \times 611.2 \times \exp\left(\frac{17.62 \times T_{Air}}{243.12 + T_{Air}} \right) \div 100, \quad \text{Eq. (6)}$$

175 The Leaf Area Index (LAI) and the Fraction of Photosynthetically Active Radiation (FPAR) were obtained from the Moderate Resolution Imaging Spectroradiometer (MODIS) Level 4 product (MCD15A3H) with a spatial resolution of 500 m and temporal resolution of 4 days (Myneni et al., 2015).

NO_x (NO/NO₂/NO_x) concentrations were monitored from 18 March to 2 June by a NO-NO₂-NO_x Trace Level Analyzer (Model 42C-TL, Thermo Fisher Scientific Inc., USA). Multipoint calibrations of NO_x were made using a NO standard gas
180 obtained from National Institute of Metrology, Beijing, China.

2.4 Stepwise multiple linear regression (MLR) model

Stepwise multiple linear regression (MLR) models were applied to identify the key environmental factors influencing O₃ deposition in the daytime (sun elevation angle > 0°) and nighttime (sun elevation angle < 0°), respectively. MLR is a commonly used approach to describe the relationship between air pollution and its influencing factors (Zhang et al., 2022b;
185 Han et al., 2020; Fu and Tai, 2015; Rannik et al., 2012). The stepwise MLR model takes the following form:

$$y = \beta_0 + \sum_{k=1}^n \beta_k x_k, \quad \text{Eq. (7)}$$

where y is the observed V_d , x_k is the selected normalized environmental parameter, β_0 is the regression constant, β_k is the regression coefficient and n is the number of selected term. β_k is determined by a forward stepwise method to add and delete terms to obtain the best model fit based on Akaike Information Criterion (AIC) statistics (Venables and Ripley, 2003).
190 Environmental parameters including seven meteorological and soil factors (T_{Air} , RH, VPD, u_* , T_{Soil} , soil VWC and PAR) and two crop related factors (LAI, FPAR) were considered during daytime, while PAR was unaccounted for during nighttime. The selected variables in the stepwise MLR were considered to be the environmental factors critical for O₃ deposition at GC during the wheat growing season.

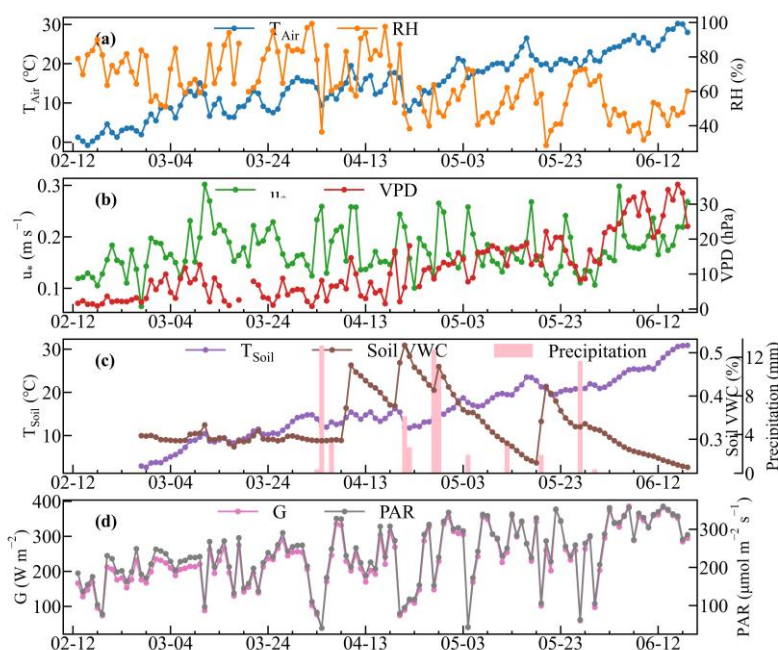
3 Results and discussion

195 3.1 Meteorological conditions

Figure 2 shows the temporal variations of daily meteorological and soil conditions during the whole period. Air and soil temperatures gradually increased from the lowest values (T_{Air} : -0.8 °C, T_{Soil} : 2.9 °C) in February to highest ones (T_{Air} : 30.2 °C, T_{Soil} : 30.9 °C) in June. RH varied around a higher level before the latter part of April and a lower level after that, with an average of 64 ± 17 %. Calculated u_* fluctuated in the range of 0.05-0.3 m s⁻¹, with an average of 0.17 ± 0.04 m s⁻¹.



200 Daily VPD was relatively stable during February-early April, with an average of 5.9 ± 4.0 hPa., and rose obviously afterwards, reaching an averaged value of 19.9 ± 7.4 hPa during May to June. Soil VWC kept flat before the middle of April and showed dramatical boosts caused by strong precipitation or irrigation events during 9-10, 20-21, 28-29 April and 19-20 May, followed by slow declines due to evapotranspiration under higher temperatures. Both PAR and G exhibited great fluctuations with slight increases from February to June.



205

Figure 2: Daily meteorological and soil conditions from 12 February to 18 June 2023: (a) T_{Air} and RH, (b) u^* and VPD, (c) precipitation, T_{Soil} and soil VWC, (d) G and PAR.

3.2 O₃ flux, deposition and concentration

Totally 2728 pairs of O₃ deposition flux and velocity were obtained for the wheat growing season, which are presented in Figure 3, along with 30-min and daily average O₃ concentrations. O₃ deposition flux averaged $-0.25 \pm 0.39 \mu\text{g m}^{-2} \text{s}^{-1}$, with a larger deposition during daytime ($-0.39 \pm 0.45 \mu\text{g m}^{-2} \text{s}^{-1}$) and a smaller one during nighttime ($-0.08 \pm 0.21 \mu\text{g m}^{-2} \text{s}^{-1}$). The largest deposition flux ($-3.20 \mu\text{g m}^{-2} \text{s}^{-1}$) was measured at the noontime of 29 April, while the largest emission flux ($0.14 \mu\text{g m}^{-2} \text{s}^{-1}$) at the midnight of 15 March. Daytime V_d averaged $0.40 \pm 0.38 \text{ cm s}^{-1}$ and was distinctly higher than nighttime ones ($0.17 \pm 0.26 \text{ cm s}^{-1}$). The averages of daytime and nighttime V_d obtained in this study were comparable to those from previous EC-based observations (0.42 cm s^{-1} and 0.14 cm s^{-1}) during the wheat growing season and higher than those (0.29 cm s^{-1} and 0.09 cm s^{-1}) during the maize growing season (Table S1) in Shangdong Province, China (Zhu et al., 2015; Zhu et al., 2014). V_d averaged $0.29 \pm 0.33 \text{ cm s}^{-1}$ over the whole observation period, ranging from -0.39 cm s^{-1} to 2.65 cm s^{-1} . The average O₃ deposition velocities observed over the wheat canopy did not show substantial differences from those previously

reported for grasslands (Mészáros et al., 2009; Coyle, 2005), forests (Wu et al., 2015; Rannik et al., 2012) and bare soil
 220 (Stella et al., 2019) (Table S1), considering the large uncertainties of reported mean values. O₃ concentrations over the wheat
 canopy were significantly enhanced after April, with an overall average of $61.8 \pm 34.6 \mu\text{g m}^{-3}$. In general, O₃ deposition
 velocities were more pronounced from mid-April to late-May (Figure 3b), when wheat was growing vigorously, while
 deposition fluxes were higher after late May due to overall higher O₃ concentration (Figure 3a, c). Thus, O₃ concentration
 was more determinative of O₃ deposition flux than V_d on longer timescales.

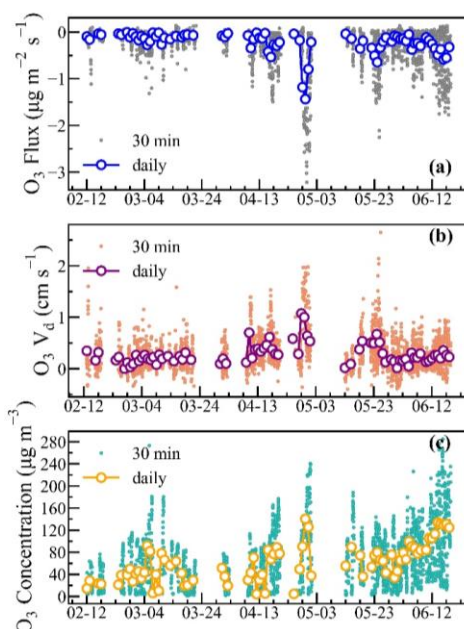
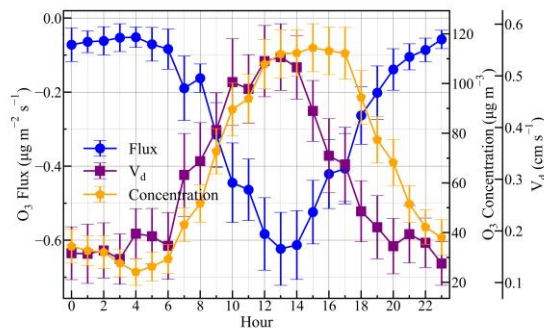


Figure 3: Timeseries of O₃ deposition flux (a), V_d (b) and concentration (c) during the wheat growing season.

The averaged diurnal patterns of O₃ deposition flux, velocity and O₃ concentration are depicted in Figure 4. With plant
 stomatal conductance and atmospheric turbulence increasing after sunrise, O₃ deposition rapidly rose during the morning
 (06:00-10:00). Deposition flux and velocity both reached their peaks ($-0.62 \mu\text{g m}^{-2} \text{s}^{-1}$ and 0.54cm s^{-1}) by 13:00, when
 230 stomatal conductance also reached a diurnal maximum (Rannik et al., 2012; Otu-Larbi et al., 2021). O₃ deposition quickly
 decreased from 14:00 to 18:00 despite of high levels of O₃ (Figure 4). Nighttime O₃ deposition remained at relatively low
 levels and exhibited weak changes, with an averaged flux and V_d of $-0.09 \pm 0.04 \mu\text{g m}^{-2} \text{s}^{-1}$ and $0.17 \pm 0.02 \text{cm s}^{-1}$,
 respectively. Therefore, diel variations in O₃ deposition over the wheat fields were mainly driven by the stomatal opening,
 with O₃ deposition velocity being decisive of deposition flux diurnal variations.

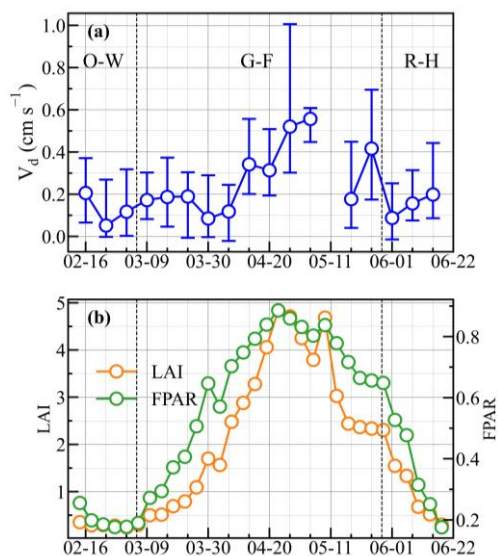


235

Figure 4: Diurnal variations of O₃ deposition flux, V_d and concentration during the wheat growing season, with error bars representing average $\pm 0.2 \times$ standard deviation values.

3.3 O₃ deposition in different stages of wheat growth

To investigate the influences of wheat growth on O₃ deposition, the entire growth season was divided into three stages:
240 Over-Wintering (O-W, 13 February-5 March), Green-Flowering (G-F, 6 March-28 May) and Ripening-Harvest (R-H, 29
May-18 June), according to the winter wheat phenology at GC (Table S2). During the O-W stage, wheat was in dormancy,
and leaves had not begun to turn green, with LAI < 0.5 (Figure 5b). V_d in the O-W stage barely changed, exhibiting a low
average of 0.20 ± 0.28 cm s⁻¹ and a median of 0.12 cm s⁻¹ (Table 1). Wheat grew vigorously in the G-F stage, with LAI
exhibiting rapid increases until the early flowering stage, after which LAI gradually decreased (Figure 5b). O₃ deposition
245 varied nearly in synchronization with LAI and wheat growth, with V_d reaching a peak when LAI exceeded 4 during the G-F
stage (Figure 5a), reaching highest daytime and nighttime averages of 0.46 ± 0.41 cm s⁻¹ and 0.24 ± 0.28 cm s⁻¹, respectively
(Table 1). Afterwards, with the maturing of wheat and the aging of leaves in the R-H stage, V_d quickly dropped back to a
low average level of 0.20 ± 0.25 cm s⁻¹, similar to that observed in the O-W stage. It can be seen that the temporal variation
of O₃ deposition velocity over wheat was predominantly determined by crop growth at GC. As for the deposition flux, both
250 the daily and daytime averaged fluxes during the G-F stage were comparable with those in the R-H stage (Table 1), which
can be attributed to the high O₃ concentrations in the summer months (Zhang et al., 2022a; Lin et al., 2009). Although
nighttime O₃ concentration during the G-F stage was also 58% lower than that in the R-H stage, nighttime O₃ deposition flux
during the G-F stage was still the highest among the three stages, which was related to the remarkably high nighttime
deposition velocities during the G-F stage (Table 1).



255

Figure 5: (a) $O_3 V_d$, (b) LAI and FPAR in different wheat growing stages. The circles and error bars in (a) denote the weekly medians and quantiles of V_d , respectively. O-W, G-F and R-H represent Over-Wintering, Green-Flowering and Ripening-Harvest stages.

Table 1: Summary of daily, daytime and nighttime $O_3 V_d$ and flux during the O-W, G-F and R-H stages.

		Over-Wintering			Green-Flowering			Ripening-Harvest		
		All	Day	Night	All	Day	Night	All	Day	Night
V_d ($cm s^{-1}$)	Mean	0.20	0.29	0.12	0.36	0.46	0.24	0.20	0.30	0.05
	Standard Deviation	0.28	0.30	0.24	0.37	0.41	0.28	0.25	0.26	0.14
	Median	0.12	0.24	0.07	0.28	0.38	0.17	0.15	0.26	0.07
	75%	0.33	0.39	0.22	0.51	0.61	0.37	0.33	0.48	0.13
	25%	0.01	0.11	-0.02	0.11	0.20	0.06	0.05	0.12	-0.01
O_3 flux ($\mu g m^{-2} s^{-1}$)	Mean	-0.10	-0.19	-0.02	-0.28	-0.42	-0.12	-0.27	-0.40	-0.06
	Standard Deviation	0.18	0.22	0.06	0.45	0.51	0.27	0.37	0.41	0.12
	Median	-0.03	-0.11	-0.01	-0.10	-0.26	-0.02	-0.12	-0.27	-0.04
	75%	0.00	-0.03	0.00	-0.01	-0.08	-0.01	-0.02	-0.08	0.00
	25%	-0.11	-0.28	-0.03	-0.36	-0.53	-0.10	-0.40	-0.62	-0.09

260

3.4 O_3 deposition relation to environmental factors



To gain deeper insights into the responses of O₃ deposition (including stomatal and non-stomatal) to environmental factors in agricultural areas, stepwise MLR models were conducted to see which factors potentially played more important roles in O₃ deposition at GC during daytime and nighttime, respectively. As shown in Table 2, RH, u*, soil VWC and LAI were identified as significant environmental factors in explaining daytime O₃ deposition changes during the entire observation period. Additionally, the coefficients of determination (R^2) of the linear model between all environmental factors and V_d was 0.46, implying that these meteorological and plant growth related factors could explain approximately 46% of the variance of daytime O₃ deposition, while R^2 was only slightly lower (0.43) with the four selected factors. Distinct key environmental factors for O₃ deposition were identified for different wheat growth stages, while LAI was only among the most important factors during the G-F stage (Table 2), confirming the significant effect of crop on O₃ deposition during its most vigorous growing stage. O₃ deposition was more sensitive to u*, soil VWC and PAR during the O-W stage, while more affected by T_{Air} and u* in the R-H stage. During nighttime, the most significant influencing factors for O₃ deposition were T_{Air}, u*, T_{Soil} and soil VWC for the whole observation period (Table 2). However, temperatures (T_{Air} and T_{Soil}) were not selected as the key factors when the stepwise MLR was separately done for the three growth stages. Compared with the R^2 of daytime MLR model, meteorological and soil conditions could explain more variance of the nighttime O₃ deposition (54%), implying that nighttime O₃ deposition processes were less complicated than daytime ones.

Table 2: Results of the MLR models for the O-W, G-F and R-H stages. Daytime MLR models represent multiple linear regression between daily average environmental variables and daytime O₃ V_d, while nighttime models represent nighttime environmental variables and V_d. The selected MLR models refer to the stepwise MLR model based on AIC statistics. Bold numbers denote those with p-value < 0.05.

	Whole Period			Over-Wintering			Green-Flowering			Ripening-Harvest		
	MLR	Selected MLR		MLR	Selected MLR		MLR	Selected MLR		MLR	Selected MLR	
	Coef.	Coef.	Std. Err.	Coef.	Coef.	Std. Err.	Coef.	Coef.	Std. Err.	Coef.	Coef.	Std. Err.
Daytime												
T _{Air}	-0.09			0.13			-0.08			0.01	0.09	0.02
RH	-0.08	-0.06	0.03	0.04			-0.07	-0.08	0.04	0.07		
u*	0.04	0.05	0.03	0.04	0.09	0.02	0.08	0.08	0.04	-0.07	-0.06	0.02
VPD	-0.06			-0.05			-0.09			0.11		
T _{Soil}	0.11			0.00			0.24			-0.21		
soil VWC	0.10	0.10	0.04	-0.01	-0.05	0.02	0.14	0.07	0.06	-0.36		
PAR	0.01			0.04	-0.04	0.04	0.05			0.03		
LAI	0.19	0.07	0.05	-0.06			0.30	0.08	0.06	0.60		
FPAR	-0.14			-0.05			-0.34			-0.45		
R ²	0.46	0.43			0.93		0.53	0.47		0.64	0.56	



Nighttime											
T _{Air}	-0.24	-0.20	0.08	0.05			-0.15			0.12	
RH	-0.07			0.08			-0.11			-0.08	-0.03 0.02
u*	0.02	0.03	0.02	-0.07			-0.01			0.02	0.03 0.02
VPD	-0.01			0.08			-0.02			-0.11	
T _{Soil}	0.20	0.18	0.06	0.20			0.12			-0.11	
soil VWC	0.12	0.12	0.02	0.15	0.07	0.02	0.11	0.12	0.02	-0.10	-0.03 0.02
R ²	0.54		0.49	0.99		0.71	0.57		0.39	0.58	0.52

Further, we explored how the selected key factors controlled the temporal variability of V_d during the three wheat growth stages (Figures 6-8). In general, the responses of both daytime and nighttime V_d to the meteorological factors were consistent throughout the entire wheat growth season (Figures 6 and 8). A clear negative impact of RH on V_d was observed at GC for daytime and nighttime (Figure 6a and 8b). Due to its negative correlation to RH (as was shown in Eq.6), high VPD was conducive to high nighttime V_d (Figure 8c). Similar response of V_d to humidity were observed over wheat and maize canopy in the NCP (Zhu et al., 2014; Zhu et al., 2015), while O_3 deposition into a boreal forest revealed strong positive correlation with RH (Rannik et al., 2012), which might be attributed from the differences in plant species and growth environment. For plants, the response of stomata to the changes of humidity is largely dependent on the plant species, plant water stress and humidity condition (Camacho et al., 1974; Rawson et al., 1977; Fanourakis et al., 2020). For example, with the increase of VPD, stomatal conductance of a tropical rainforest gradually increased (Mendes and Marengo, 2017), while the leaf diffusion resistance of sesame also increased markedly (Camacho et al., 1974). Thus, the similar change of humidity might have opposite effect on O_3 deposition over different canopies. Besides, O_3 deposition processes also varied with the humidity. Under dry condition (RH < 60%), O_3 deposition over crop canopy is significantly controlled by stomatal uptake; above 60-70% RH, a thin liquid film on leaf surface will block dry deposition but enhance the aqueous reactions of O_3 , thus the contribution of non-stomatal deposition is higher and more variable (Coyle et al., 2009; Lamaud et al., 2009). Strong turbulence (represented by elevated u_*) can transport O_3 more efficiently to the surface (Cape et al., 2009), thus V_d almost linearly increased with u_* (Figure 6b and 8d). The sensitivity of V_d to u_* was also affected by LAI, with daytime V_d under similar levels of u_* being significantly higher under higher LAI (Figure 7a and Table S3). High LAI indicates dense vegetation coverage and potential large stomatal conductance, which can provide more active (stomatal and cuticular) areas for the uptake of O_3 , further promoting O_3 deposition. PAR had a positive effect on O_3 deposition during the observation period (Figure 6c). On the one side, increasing PAR induces automatic leaf stomatal opening thereby determining stomatal conductance and net photosynthesis (Yu et al., 2004), affecting the stomatal O_3 uptake (Tong et al., 2015). On the other side, PAR (also reflecting radiation intensity) affects O_3 photochemistry directly by accelerating atmospheric photolysis reactions both above and within the canopy and indirectly by influencing the emission of biogenic VOCs (Yang et al., 2021; Van



Meeningen et al., 2017; Yuan et al., 2016), thus disturbing the distributions of O_3 and its precursors and contributing non-stomatal O_3 fluxes with surface processes (Fares et al., 2008; Cape et al., 2009). Positive dependences of V_d on u^* and PAR were observed over other crop fields (such as wheat, maize, and potato) (Coyle et al., 2009; Zhu et al., 2014; Zhu et al., 2015). In addition, both T_{Air} and T_{Soil} exhibited weak relationships with nighttime V_d (Figures 8a, e), which were different from the reported positive correlations between temperature and V_d (Coyle et al., 2009; Rannik et al., 2012). These imply the variability and complexity of O_3 deposition affected by the combined influences of various environmental factors.

During the O-W and R-H stage, soil VWC was at relatively lower levels. During the G-F stage, soil VWC reached beyond 0.30% and V_d rose significantly with rising soil VWC (Figure 6d and 8f). Although soil moisture blocks the diffusion of O_3 in soil and reduces reactive spaces for O_3 absorption, suppressing O_3 soil deposition (Stella et al., 2011), it can also promote total O_3 deposition through several indirect pathways. From the plant physiological aspect, stomatal conductance and plant net photosynthesis are both promoted by higher soil VWC (Otu-Larbi et al., 2021; Anav et al., 2018; Medlyn et al., 2011; Jarvis et al., 1997; Ball et al., 1987). Stomatal conductance revealed overshoots after the watering of dry soil, accordingly, significantly increased transpiration and photosynthesis of crops or vegetation were detected (Wu et al., 2021; Reich et al., 2018; Ramírez et al., 2018; Rawson and Clarke, 1988; Popescu, 1967). This effect was reflected at GC by the more obvious response of V_d to soil VWC changes under higher LAI (Figure 7b and Table S3), confirming again that O_3 deposition during the G-F stage was mainly driven by stomatal deposition, rather than soil deposition. Consequently, soil VWC revealed positive coefficients in the MLR models for the G-F period at GC. Our result is qualitatively consistent with the observation based estimation of stomatal and soil O_3 deposition relative contributions over a wheat canopy in Nanjing city, China, which accounted for 41.2% and 15.4%, respectively (Xu et al., 2018).

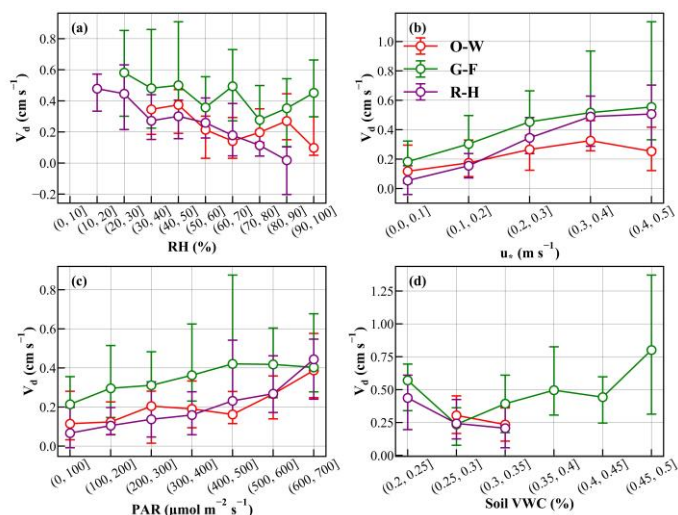
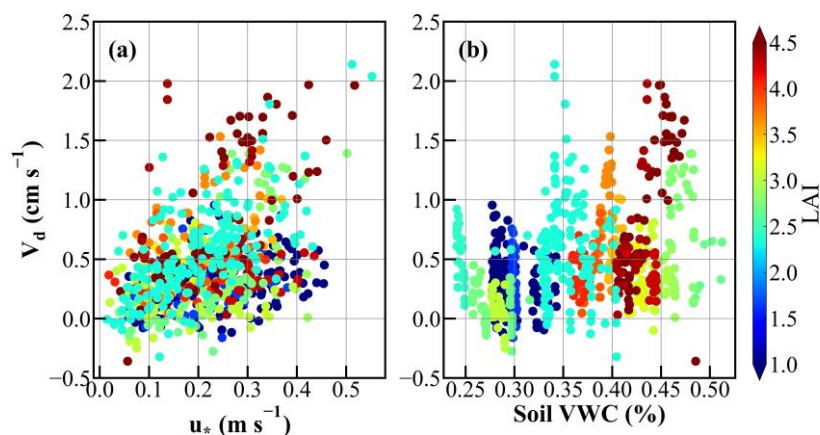


Figure 6: Dependences of daytime O_3 V_d on (a) RH, (b) u^* , (c) PAR and (d) soil VWC during the O-W, G-F and R-H stages. Medians of 30-min V_d with quartiles are presented.



330 **Figure 7: The variation of daytime V_d with (a) u_* , (b) soil VWC under changing LAI during the G-F stage.**

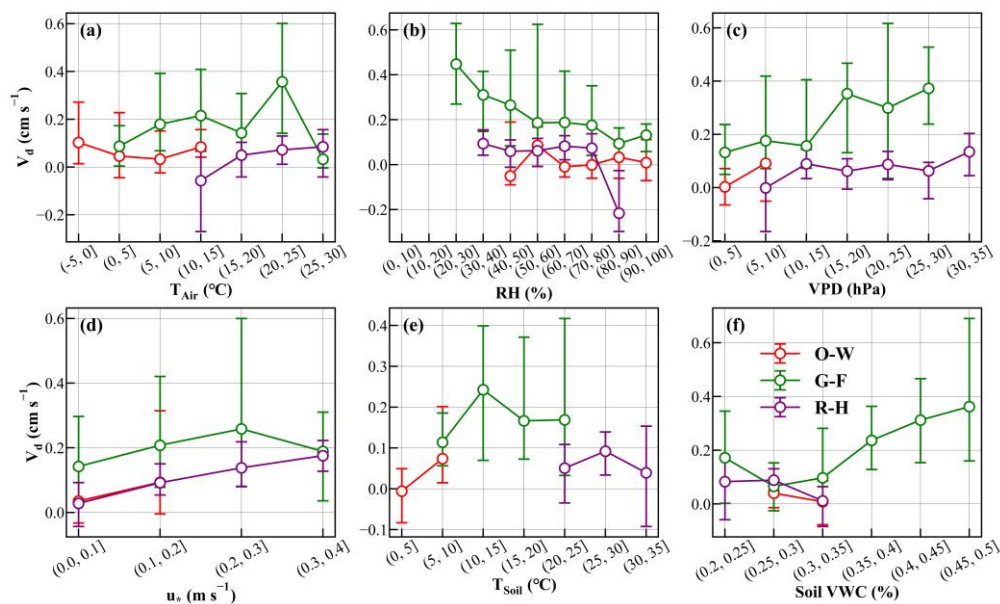


Figure 8: Dependences of $O_3 V_d$ on (a) T_{Air} , (b) RH, (c) VPD, (d) u_* , (e) T_{Soil} and (f) soil VWC in the nighttime during the O-W, G-F and R-H stages. Medians of 30-min V_d with quartiles are presented.

335 Overall, soil VWC at GC kept low expect for four abrupt increasing events that occurred during the G-F stage, with the highest soil VWC reaching 0.55% (Figure 2c). The three most prominent episodes induced by farm field irrigation were more thoroughly investigated to uncover how soil moisture affected O_3 deposition at GC. Interestingly, simultaneous increments in V_d were detected upon the increase of soil VWC, with V_d being distinctly elevated within days afterwards (Figure 9). Soil VWC increased from 0.32% to 0.51% at noontime on 9 April, and V_d rapidly rose from 0.16 to 0.64 $cm s^{-1}$ at the same time. Dramatic increments in both averaged nighttime and daytime V_d were detected on the following days. During



340 nighttime, V_d reached an average of 0.30 cm s^{-1} , significantly higher than the average daytime level (0.18 cm s^{-1}) on 9 April, and a maximum of 0.76 cm s^{-1} , which also exceeded the maximum of 0.64 cm s^{-1} observed during the daytime of 9 April (Figure 9a). The dramatic rise in V_d on 10 April resulted a 317% increase in daytime O_3 deposition flux (from $0.12 \mu\text{g m}^{-2} \text{ s}^{-1}$ to $0.50 \mu\text{g m}^{-2} \text{ s}^{-1}$), with only a small change in daytime O_3 concentration from 9 April ($41.4 \mu\text{g m}^{-3}$) to 10 April ($48.2 \mu\text{g m}^{-3}$, Figure S4a). In addition, drastic elevations in V_d during the night and morning periods were also observed following other
345 episodes of sudden increases in soil VWC (Figure 9b, c). Similar enhancements and disrupted daily cycles of O_3 deposition were also observed over the canopy of a pine forest during rainfall events (Altimir et al., 2006).

Considering the direct effect of soil moisture on plant physiology, the temporal variations of CO_2 and H_2O fluxes were examined to characterize changes in transpiration and photosynthesis of wheat affected by the abrupt increases of soil water contents. As shown in Figure 10, both CO_2 and H_2O fluxes exhibited obvious increases on the days following the soil VWC
350 increments. The daily peaks of H_2O fluxes increased from 0.08 to $0.13 \text{ g m}^{-2} \text{ s}^{-1}$ between 9 and 10 April and from 0.12 to $0.19 \text{ g m}^{-2} \text{ s}^{-1}$ between 28 and 29 April, respectively, while daily averaged CO_2 fluxes before and after the abrupt increasing events rose from $0.28 \text{ mg m}^{-2} \text{ s}^{-1}$ to $0.55 \text{ mg m}^{-2} \text{ s}^{-1}$ and $0.51 \text{ mg m}^{-2} \text{ s}^{-1}$ to $0.55 \text{ mg m}^{-2} \text{ s}^{-1}$, respectively (Figure 10a, b). Subsequently, CO_2 and H_2O fluxes, as well as V_d of O_3 exhibited declines with the slow loss in soil moisture (Figure 9 and 10). This indicates that transpiration and photosynthesis of wheat were sharply enhanced after soil water contents increased,
355 leading to larger leaf stomatal conductance and strengthening O_3 stomatal uptake. These results were consistent with those obtained in previous conditional control experiments and field observations (Wu et al., 2021; Reich et al., 2018; Ramírez et al., 2018; Rawson and Clarke, 1988; Popescu, 1967). In addition, moist soil can extend the time window of wheat leaves' stomatal opening, both in the hours after sunset and before dawn (Schoppach et al., 2020; Ramírez et al., 2018). Stomata can even stay open during nighttime after precipitation or irrigation events (Kobayashi et al., 2007; Rawson and Clarke, 1988).
360 During the irrigation induced high soil VWC episodes, positive H_2O fluxes were also observed at GC during the night, such as on 10 April and 28 April (Figure 10a, b), implying that wheat transpiration might not stop over the night and that leaf stomata might have not completely closed, continuing to uptake O_3 at night, significantly enhancing nocturnal O_3 deposition.

Additionally, the high nighttime O_3 deposition (V_d) phenomenon was always accompanied by positive water vapor fluxes and high NO concentrations, and occurred mainly after the rapid increase of soil VWC (Figure S5). As shown in Figure 9,
365 high NO became more frequent at night during the high soil VWC events, and nighttime V_d dramatically increased when NO fluctuated at obviously high levels and nighttime O_3 concentration was still at low level (Figure S4). This might be attributable to the fact that soil NO emissions were promoted by the watering process, as soil water content is a decisive factor for the transformation and emission of reactive nitrogen within soils (Schindlbacher et al., 2004; Ghude et al., 2010; Kim et al., 2012; Weber et al., 2015; Zörner et al., 2016). Enhanced nighttime soil NO emissions may inevitably cause
370 stronger NO titration with O_3 within wheat canopy, facilitating the non-stomatal O_3 deposition at night.

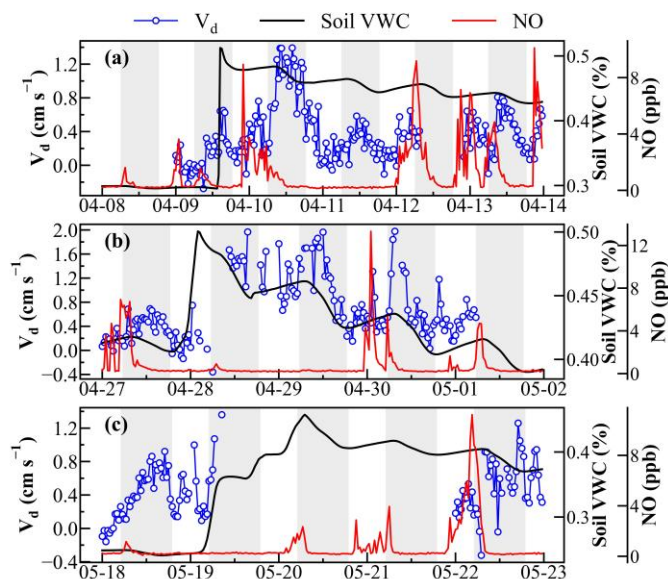
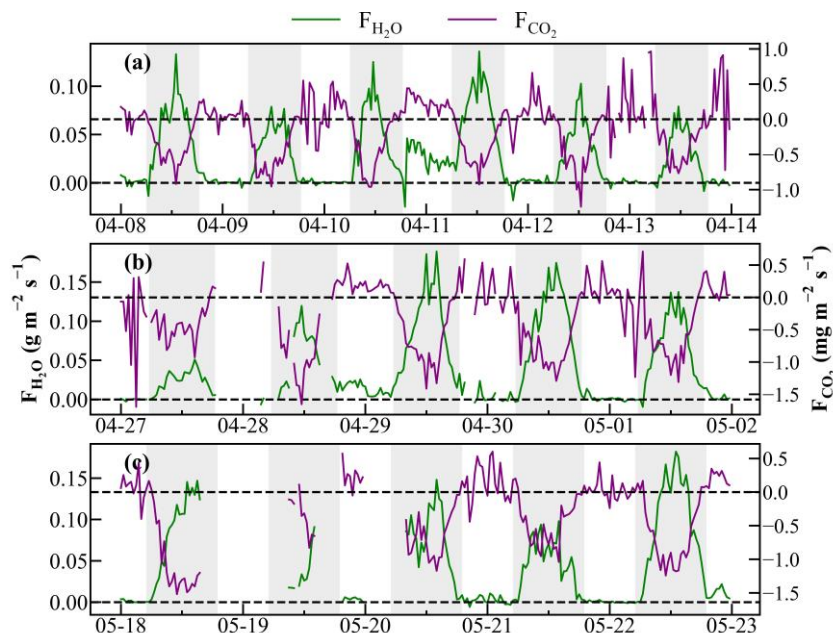


Figure 9: Variations of O_3 V_d (blue circle lines), soil VWC (black lines) and NO concentration (red lines) during 8-13 April (a), 27 April-1 May (b) and 18-22 May (c). The shades represent the daytime.



375 **Figure 10:** Variations of H_2O flux (F_{H_2O} , green lines) and CO_2 flux (F_{CO_2} , purple lines) during (a) 8-13 April, (b) 27 April-1 May and (c) 18-22 May, with shades representing daytime hours.

In summary, both daytime and nighttime O_3 deposition fluxes and V_d were significantly affected by environmental conditions, through stomatal and nonstomatal pathways, with crop growth playing a critical role. Abrupt increments in soil



380 moisture induced dramatic changes in V_d , which not only altered the diurnal cycle of O_3 deposition, but also caused large fluctuations in averaged O_3 deposition flux on longer timescales.

4 Conclusions and implications

In this study, we developed a relaxed eddy accumulation (REA) O_3 flux measurement system, verified its reliability, and conducted measurements of O_3 deposition using this newly developed REA system over the wheat canopy at a polluted agricultural site (GC) in the NCP during the main wheat growing season. We also collected ancillary data related to O_3 deposition and tried to make an integrated analysis. The observed O_3 deposition flux and velocity over the wheat fields at GC averaged $-0.25 \pm 0.39 \mu\text{g m}^{-2} \text{s}^{-1}$ and $0.29 \pm 0.33 \text{ cm s}^{-1}$, respectively. The diurnal cycle of V_d was controlled by the crop stomatal opening during the day. Daytime V_d ($0.40 \pm 0.38 \text{ cm s}^{-1}$) was obviously higher than nighttime one ($0.17 \pm 0.26 \text{ cm s}^{-1}$). V_d played a decisive role in the diel pattern of O_3 deposition flux, while O_3 concentration determined the flux variability on the longer timescales. The temporal changes of V_d were synchronous with the evolutions of LAI and wheat growth, suggesting the determining effect of crops on O_3 uptake and the predominant contribution of stomatal uptake to the overall O_3 deposition. During the wheat growth season, RH, u_* , soil VWC and LAI were identified as the most significant factors in explaining the changes of O_3 deposition in the daytime, while u_* and soil VWC were more important in the nighttime. V_d exhibited significant increases with the decrease of RH and increases of u_* , PAR and soil VWC, which were enhanced by higher LAI. With the rapid increases of soil VWC after strong precipitation or irrigation events, stomatal conductance increased and stomatal opening extended to nighttime hours, enhancing transpiration and photosynthesis of wheat, which remarkably strengthened O_3 stomatal uptake during daytime and nighttime. Meanwhile, soil NO emission might have also been strengthened under moist soil conditions, which facilitated NO titration of O_3 within the canopy and enhanced non-stomatal O_3 removals at night. Therefore, drastically increasing soil moisture led to the dramatic and simultaneous increments in V_d .

400 Observations have proved the dominant effects of crop growth on O_3 deposition processes over wheat fields during its growth season, whereas the actual relative contributions of crops to O_3 deposition through different pathways need to be further quantified. On the other hand, the influences of crops on O_3 deposition through stomatal uptake or surface removal have been investigated in extensive studies (Ainsworth, 2017; Aunan et al., 2000; Bender and Weigel, 2011; Biswas et al., 2008; Epa, 2013; Felzer et al., 2005; Harmens et al., 2018; Piikki et al., 2008). How much impact will O_3 deposition have on crop growth and yield under the currently severe O_3 pollution with significant upward trends in the NCP remains an unsolved issue. Although many researches have assessed the crop yield loss caused by O_3 pollution based on exposure-response functions (Feng et al., 2019a; Hu et al., 2020; Feng et al., 2020), the concentration-based evaluation was less related to the actual exposure than deposition flux (Zhu et al., 2015). Therefore, more accurate quantification of agricultural impacts induced by O_3 (based on O_3 deposition fluxes) are required in future studies.



410 During the wheat growth season, the temporal variation of O_3 deposition velocity fluctuated greatly with changes in
environmental conditions, and the dominant factors determining the V_d variability varied with the growth stages of wheat.
Meanwhile, the key influencing factors and their effects on O_3 deposition varied with different canopy and ground surface.
Beside environmental conditions, agricultural activities also significantly affected O_3 deposition (Mészáros et al., 2009).
Thus, using a unanimous O_3 deposition parameterization scheme on different plant canopies/surfaces or throughout distinct
415 growth stages might cause large errors in simulation results, explaining the large discrepancies between modelled and
observed O_3 dry deposition fluxes in the growth seasons (Clifton et al., 2020b; Hardacre et al., 2015). More O_3 deposition
observations over different land surfaces are definitely needed in the future, both facilitating the O_3 dry deposition
mechanism exploration and model optimization.

Finally, abrupt increases in soil moisture during strong precipitation and irrigation resulted in dramatic and overall
420 increases in V_d over the wheat fields, and extremely high nighttime V_d was observed, affecting the total O_3 deposition.
Impacted by climate warming, more frequent irrigation in agricultural areas might promote O_3 deposition following the drier
and hotter days, when the photochemical production of O_3 is greatly enhanced and O_3 concentration is at a high level (Yuan
et al., 2016; Lu et al., 2019). Meanwhile, increasing temperature promotes the emissions of soil NO and biogenic VOCs (Ma
et al., 2019; Lu et al., 2020), further facilitating O_3 production and deposition. Correspondingly, the feedback of these
425 climate-related impacts on the vegetation growth is worth further study. On the other hand, the processes of stomatal opening
and transpiration have been commonly assumed to occur during daytime and stop during the night. However, more and more
studies have showed the non-negligible effects of nocturnal unclosed stomatal and transpiration for a wide range of plant
species (Kukal and Irmak, 2022; Schoppach et al., 2020; Tamang et al., 2019; Ramírez et al., 2018; Hoshika et al., 2018),
and the viable breeding target on increasing pre-dawn circadian control would be set to alleviate the adverse effect of
430 increasing drought under climate warming (Schoppach et al., 2020). With the significant increasing O_3 levels in China,
nighttime O_3 concentration and exposure also exhibited upward trend in recent years (Agathokleous et al., 2023; He et al.,
2022). How nocturnal plant activities and rising nighttime O_3 concentration interact with each other is worth deeper
investigation.

Data availability

435 The data used in this study are available from the corresponding authors upon request.

Author contributions

XY and WX designed the experiment and XB led the research. XY made the O_3 deposition measurement with the help of
WL, WX, ZG, XB and JM. JJ, ZL, SX, HR and GS were responsible for the EC flux measurement. XY analyzed the data
and wrote the paper with help of WL, WX, XB.



440 Competing interest

The authors have no competing interests to declare.

Acknowledgments

This work is supported by the National Natural Science Foundation of China (42175127 and 41875159), Beijing Natural Science Foundation (8222078), CAMS projects (2023Z012 and 2020KJ003).

445 References

- Agathokleous, E., Feng, Z., and Sicard, P.: Surge in nocturnal ozone pollution, *Science*, 382, 1131-1131, 10.1126/science.adm7628, 2023.
- Ainsworth, E. A.: Understanding and improving global crop response to ozone pollution, *The Plant Journal*, 90, 886-897, <https://doi.org/10.1111/tjp.13298>, 2017.
- Altimir, N., Kolari, P., Tuovinen, J. P., Vesala, T., Bäck, J., Suni, T., Kulmala, M., and Hari, P.: Foliage surface ozone deposition: a role for surface moisture?, *Biogeosciences*, 3, 209-228, 10.5194/bg-3-209-2006, 2006.
- Anav, A., Proietti, C., Menut, L., Carnicelli, S., De Marco, A., and Paoletti, E.: Sensitivity of stomatal conductance to soil moisture: implications for tropospheric ozone, *Atmos. Chem. Phys.*, 18, 5747-5763, 10.5194/acp-18-5747-2018, 2018.
- Aunan, K., Berntsen, T., and Seip, H.: Surface Ozone in China and its Possible Impact on Agricultural Crop Yields, *Ambio*, 29, 10.1639/0044-7447(2000)029[0294:SOICAI]2.0.CO;2, 2000.
- 455 Baldocchi, D.: A Multi-layer model for estimating sulfur dioxide deposition to a deciduous oak forest canopy, *Atmospheric Environment* (1967), 22, 869-884, [https://doi.org/10.1016/0004-6981\(88\)90264-8](https://doi.org/10.1016/0004-6981(88)90264-8), 1988.
- Baldocchi, D. D., Hincks, B. B., and Meyers, T. P.: Measuring Biosphere-Atmosphere Exchanges of Biologically Related Gases with Micrometeorological Methods, *Ecology*, 69, 1331-1340, <https://doi.org/10.2307/1941631>, 1988.
- 460 Ball, J. T., Woodrow, I. E., and Berry, J. A.: A Model Predicting Stomatal Conductance and its Contribution to the Control of Photosynthesis under Different Environmental Conditions, in: *Progress in Photosynthesis Research: Volume 4 Proceedings of the VIIth International Congress on Photosynthesis Providence, Rhode Island, USA, August 10–15, 1986*, edited by: Biggins, J., Springer Netherlands, Dordrecht, 221-224, 10.1007/978-94-017-0519-6_48, 1987.
- Bender, J. and Weigel, H.-J.: Changes in atmospheric chemistry and crop health: A review, *Agronomy for Sustainable Development*, 31, 81, 10.1051/agro/2010013, 2011.
- 465 Biswas, D. K., Xu, H., Li, Y. G., Sun, J. Z., Wang, X. Z., Han, X. G., and Jiang, G. M.: Genotypic differences in leaf biochemical, physiological and growth responses to ozone in 20 winter wheat cultivars released over the past 60 years, *Global Change Biology*, 14, 46-59, <https://doi.org/10.1111/j.1365-2486.2007.01477.x>, 2008.
- Bowling, D. R., Delany, A. C., Turnipseed, A. A., Baldocchi, D. D., and Monson, R. K.: Modification of the relaxed eddy accumulation technique to maximize measured scalar mixing ratio differences in updrafts and downdrafts, *J. Geophys. Res. Atmos.*, 104, 9121-9133, <https://doi.org/10.1029/1999JD900013>, 1999.
- 470 Businger, J. A.: Evaluation of the Accuracy with Which Dry Deposition Can Be Measured with Current Micrometeorological Techniques, *Journal of Applied Meteorology and Climatology*, 25, 1100-1124, 10.1175/1520-0450(1986)025<1100:EOTAWW>2.0.CO;2, 1986.
- Businger, J. A. and Oncley, S. P.: Flux Measurement with Conditional Sampling, *Journal of Atmospheric and Oceanic Technology*, 7, 349-352, 10.1175/1520-0426(1990)007<0349:FMWCS>2.0.CO;2, 1990.
- 475 Camacho, B. S., Hall, A. E., and Kaufmann, M. R.: Efficiency and regulation of water transport in some woody and herbaceous species, *Plant Physiol.*, 54, 169-172, 10.1104/pp.54.2.169, 1974.
- Cape, J. N., Hamilton, R., and Heal, M. R.: Reactive uptake of ozone at simulated leaf surfaces: Implications for 'non-stomatal' ozone flux, *Atmos. Environ.*, 43, 1116-1123, <https://doi.org/10.1016/j.atmosenv.2008.11.007>, 2009.
- 480 Clifton, O. E., Paulot, F., Fiore, A. M., Horowitz, L. W., Correa, G., Baublitz, C. B., Fares, S., Goded, I., Goldstein, A. H., Gruening, C., Hogg, A. J., Loubet, B., Mammarella, I., Munger, J. W., Neil, L., Stella, P., Uddling, J., Vesala, T., and Weng, E.: Influence of Dynamic Ozone Dry Deposition on Ozone Pollution, *J. Geophys. Res. Atmos.*, 125, e2020JD032398, <https://doi.org/10.1029/2020JD032398>, 2020a.
- Clifton, O. E., Fiore, A. M., Massman, W. J., Baublitz, C. B., Coyle, M., Emberson, L., Fares, S., Farmer, D. K., Gentine, P., Gerosa, G., Guenther, A. B., Helmig, D., Lombardozzi, D. L., Munger, J. W., Patton, E. G., Pusede, S. E., Schwede, D. B., Silva, S. J., Sörgel, M., Steiner, A. L., and Tai, A. P. K.: Dry Deposition of Ozone Over Land: Processes, Measurement, and Modeling, *Reviews of Geophysics*, 58, e2019RG000670, <https://doi.org/10.1029/2019RG000670>, 2020b.
- 485



- Coyle, M.: The gaseous exchange of ozone at terrestrial surfaces : non-stomatal deposition to grassland, Coyle, M., Nemitz, E., Storeton-West, R., Fowler, D., and Cape, J. N.: Measurements of ozone deposition to a potato canopy, *Agricultural and Forest Meteorology*, 149, 655-666, <https://doi.org/10.1016/j.agrformet.2008.10.020>, 2009.
- Desjardins, R. L.: Description and evaluation of a sensible heat flux detector, *Boundary-Layer Meteorology*, 11, 147-154, 10.1007/BF02166801, 1977.
- 490 Dong, C., Gao, R., Zhang, X., Li, H., Wang, W., and Xue, L.: Assessment of O₃-induced crop yield losses in northern China during 2013–2018 using high-resolution air quality reanalysis data, *Atmos. Environ.*, 259, 118527, <https://doi.org/10.1016/j.atmosenv.2021.118527>, 2021.
- EPA: Integrated Science Assessment (ISA) for Ozone and Related Photochemical Oxidants (Final Report, Feb 2013), Environmental Protection Agency, Washington, DC, U.S.2013.
- 495 Fanourakis, D., Aliniaiefard, S., Sellin, A., Giday, H., Körner, O., Rezaei Nejad, A., Delis, C., Bouranis, D., Koubouris, G., Kambourakis, E., Nikoloudakis, N., and Tsaniklidis, G.: Stomatal behavior following mid- or long-term exposure to high relative air humidity: A review, *Plant Physiology and Biochemistry*, 153, 92-105, <https://doi.org/10.1016/j.plaphy.2020.05.024>, 2020.
- Fares, S., Loreto, F., Kleist, E., and Wildt, J.: Stomatal uptake and stomatal deposition of ozone in isoprene and monoterpene emitting plants, *Plant Biology*, 10, 44-54, <https://doi.org/10.1055/s-2007-965257>, 2008.
- 500 Felzer, B., Reilly, J., Melillo, J., Kicklighter, D., Sarofim, M., Wang, C., Prinn, R., and Zhuang, Q.: Future Effects of Ozone on Carbon Sequestration and Climate Change Policy Using a Global Biogeochemical Model, *Climatic Change*, 73, 345-373, 10.1007/s10584-005-6776-4, 2005.
- Feng, Z., Hu, T., Tai, A. P. K., and Calatayud, V.: Yield and economic losses in maize caused by ambient ozone in the North China Plain (2014–2017), *Sci.Total Environ.*, 722, 137958, <https://doi.org/10.1016/j.scitotenv.2020.137958>, 2020.
- 505 Feng, Z., Kobayashi, K., Li, P., Xu, Y., Tang, H., Guo, A., Paoletti, E., and Calatayud, V.: Impacts of current ozone pollution on wheat yield in China as estimated with observed ozone, meteorology and day of flowering, *Atmos. Environ.*, 217, 116945, <https://doi.org/10.1016/j.atmosenv.2019.116945>, 2019a.
- Feng, Z., De Marco, A., Anav, A., Gualtieri, M., Sicard, P., Tian, H., Fornasier, F., Tao, F., Guo, A., and Paoletti, E.: Economic losses due to ozone impacts on human health, forest productivity and crop yield across China, *Environ. Int.*, 131, 104966, <https://doi.org/10.1016/j.envint.2019.104966>, 2019b.
- Fowler, D., Flechard, C., Cape, J. N., Storeton-West, R. L., and Coyle, M.: Measurements of Ozone Deposition to Vegetation Quantifying the Flux, the Stomatal and Non-Stomatal Components, *Water, Air, and Soil Pollution*, 130, 63-74, 10.1023/A:1012243317471, 2001.
- 515 Fu, Y. and Tai, A. P. K.: Impact of climate and land cover changes on tropospheric ozone air quality and public health in East Asia between 1980 and 2010, *Atmos. Chem. Phys.*, 15, 10093-10106, 10.5194/acp-15-10093-2015, 2015.
- Ghude, S. D., Lal, D. M., Beig, G., van der A, R., and Sable, D.: Rain-Induced Soil NO_x Emission From India During the Onset of the Summer Monsoon: A Satellite Perspective, *J. Geophys. Res. Atmos.*, 115, <https://doi.org/10.1029/2009JD013367>, 2010.
- Grelle, A. and Keck, H.: Affordable relaxed eddy accumulation system to measure fluxes of H₂O, CO₂, CH₄ and N₂O from ecosystems, *Agricultural and Forest Meteorology*, 307, 108514, <https://doi.org/10.1016/j.agrformet.2021.108514>, 2021.
- 520 Han, H., Liu, J., Shu, L., Wang, T., and Yuan, H.: Local and synoptic meteorological influences on daily variability in summertime surface ozone in eastern China, *Atmospheric Chemistry Physics*, 20, 203-222, 10.5194/acp-20-203-2020, 2020.
- Hardacre, C., Wild, O., and Emberson, L.: An evaluation of ozone dry deposition in global scale chemistry climate models, *Atmos. Chem. Phys.*, 15, 6419-6436, 10.5194/acp-15-6419-2015, 2015.
- Harmens, H., Hayes, F., Mills, G., Sharps, K., Osborne, S., and Pleijel, H.: Wheat yield responses to stomatal uptake of ozone: Peak vs rising background ozone conditions, *Atmos. Environ.*, 173, 1-5, <https://doi.org/10.1016/j.atmosenv.2017.10.059>, 2018.
- 525 He, C., Lu, X., Wang, H., Wang, H., Li, Y., He, G., He, Y., Wang, Y., Zhang, Y., Liu, Y., Fan, Q., and Fan, S.: The unexpected high frequency of nocturnal surface ozone enhancement events over China: characteristics and mechanisms, *Atmos. Chem. Phys.*, 22, 15243-15261, 10.5194/acp-22-15243-2022, 2022.
- Held, A., Patton, E., Rizzo, L., Smith, J., Turnipseed, A., and Guenther, A.: Relaxed Eddy Accumulation Simulations of Aerosol Number Fluxes and Potential Proxy Scalars, *Boundary-Layer Meteorology*, 129, 451-468, 10.1007/s10546-008-9327-5, 2008.
- 530 Helmig, D., Lang, E. K., Bariteau, L., Boylan, P., Fairall, C. W., Ganzeveld, L., Hare, J. E., Hueber, J., and Pallandt, M.: Atmosphere-ocean ozone fluxes during the TexAQS 2006, STRATUS 2006, GOMECC 2007, GasEx 2008, and AMMA 2008 cruises, *J. Geophys. Res. Atmos.*, 117, <https://doi.org/10.1029/2011JD015955>, 2012.
- Hicks, B. B. and Wesely, M. L.: An examination of some micrometeorological methods for measuring dry deposition, EPA Interagency Energy/Environment R&D Program Report, a, EPA-600/607-678-116, 1978.
- 535 Hoshika, Y., Osada, Y., de Marco, A., Peñuelas, J., and Paoletti, E.: Global diurnal and nocturnal parameters of stomatal conductance in woody plants and major crops, *Global Ecology and Biogeography*, 27, 257-275, <https://doi.org/10.1111/geb.12681>, 2018.
- Hu, T., Liu, S., Xu, Y., Feng, Z., and Calatayud, V.: Assessment of O₃-induced yield and economic losses for wheat in the North China Plain from 2014 to 2017, *China, Environ. Pollut.*, 258, 113828, <https://doi.org/10.1016/j.envpol.2019.113828>, 2020.



- 540 Jarvis, P. G., Monteith, J. L., and Weatherley, P. E.: The interpretation of the variations in leaf water potential and stomatal conductance found in canopies in the field, *Philosophical Transactions of the Royal Society of London. B, Biological Sciences*, 273, 593-610, 10.1098/rstb.1976.0035, 1997.
- Kim, D. G., Vargas, R., Bond-Lamberty, B., and Turetsky, M. R.: Effects of soil rewetting and thawing on soil gas fluxes: a review of current literature and suggestions for future research, *Biogeosciences*, 9, 2459-2483, 10.5194/bg-9-2459-2012, 2012.
- 545 Kobayashi, N., Hiyama, T., Fukushima, Y., Lopez, M. L., Hirano, T., and Fujinuma, Y.: Nighttime transpiration observed over a larch forest in Hokkaido, Japan, *Water Resources Research*, 43, <https://doi.org/10.1029/2006WR005556>, 2007.
- Kuang, Y., Xu, W., Lin, W., Meng, Z., Zhao, H., Ren, S., Zhang, G., Liang, L., and Xu, X.: Explosive morning growth phenomena of NH₃ on the North China Plain: Causes and potential impacts on aerosol formation, *Environ. Pollut.*, 257, 113621, <https://doi.org/10.1016/j.envpol.2019.113621>, 2020.
- 550 Kukal, M. S. and Irmak, S.: Nocturnal transpiration in field crops: Implications for temporal aggregation and diurnal weighing of vapor pressure deficit, *Agricultural Water Management*, 266, 107578, <https://doi.org/10.1016/j.agwat.2022.107578>, 2022.
- Lamaud, E., Loubet, B., Irvine, M., Stella, P., Personne, E., and Cellier, P.: Partitioning of ozone deposition over a developed maize crop between stomatal and non-stomatal uptakes, using eddy-covariance flux measurements and modelling, *Agricultural and Forest Meteorology*, 149, 1385-1396, <https://doi.org/10.1016/j.agrformet.2009.03.017>, 2009.
- 555 Lelieveld, J. and Dentener, F. J.: What controls tropospheric ozone?, *J. Geophys. Res. Atmos.*, 105, 3531-3551, 10.1029/1999JD901011, 2000.
- Li, K., Jacob, D. J., Liao, H., Shen, L., Zhang, Q., and Bates, K. H.: Anthropogenic drivers of 2013–2017 trends in summer surface ozone in China, *P. Natl. Acad. Sci.*, 116, 422, 10.1073/pnas.1812168116, 2019.
- Lin, W., Xu, X., Ge, B., and Zhang, X.: Characteristics of gaseous pollutants at Gucheng, a rural site southwest of Beijing, *J. Geophys. Res. Atmos.*, 114, <https://doi.org/10.1029/2008JD010339>, 2009.
- 560 Loubet, B., Cellier, P., Fléclard, C., Zurfluh, O., Irvine, M., Lamaud, E., Stella, P., Roche, R., Durand, B., Flura, D., Masson, S., Laville, P., Garrigou, D., Personne, E., Chelle, M., and Castell, J.-F.: Investigating discrepancies in heat, CO₂ fluxes and O₃ deposition velocity over maize as measured by the eddy-covariance and the aerodynamic gradient methods, *Agricultural and Forest Meteorology*, 169, 35-50, <https://doi.org/10.1016/j.agrformet.2012.09.010>, 2013.
- 565 Lu, X., Zhang, L., Wang, X., Gao, M., Li, K., Zhang, Y., Yue, X., and Zhang, Y.: Rapid Increases in Warm-Season Surface Ozone and Resulting Health Impact in China Since 2013, *Environmental Science & Technology Letters*, 7, 240-247, <https://doi.org/10.1021/acs.estlett.0c00171>, 2020.
- Lu, X., Zhang, L., Chen, Y., Zhou, M., Zheng, B., Li, K., Liu, Y., Lin, J., Fu, T. M., and Zhang, Q.: Exploring 2016–2017 surface ozone pollution over China: source contributions and meteorological influences, *Atmos. Chem. Phys.*, 19, 8339-8361, 10.5194/acp-19-8339-2019, 2019.
- 570 Lyu, X., Li, K., Guo, H., Morawska, L., Zhou, B., Zeren, Y., Jiang, F., Chen, C., Goldstein, A. H., Xu, X., Wang, T., Lu, X., Zhu, T., Querol, X., Chatani, S., Latif, M. T., Schuch, D., Sinha, V., Kumar, P., Mullins, B., Seguel, R., Shao, M., Xue, L., Wang, N., Chen, J., Gao, J., Chai, F., Simpson, I., Sinha, B., and Blake, D. R.: A synergistic ozone-climate control to address emerging ozone pollution challenges, *One Earth*, 6, 964-977, <https://doi.org/10.1016/j.oneear.2023.07.004>, 2023.
- 575 Ma, M., Gao, Y., Wang, Y., Zhang, S., Leung, L. R., Liu, C., Wang, S., Zhao, B., Chang, X., Su, H., Zhang, T., Sheng, L., Yao, X., and Gao, H.: Substantial ozone enhancement over the North China Plain from increased biogenic emissions due to heat waves and land cover in summer 2017, *Atmos. Chem. Phys.*, 19, 12195-12207, 10.5194/acp-19-12195-2019, 2019.
- Ma, Z., Xu, J., Quan, W., Zhang, Z., Lin, W., and Xu, X.: Significant increase of surface ozone at a rural site, north of eastern China, *Atmos. Chem. Phys.*, 16, 3969-3977, 10.5194/acp-16-3969-2016, 2016.
- 580 Matsuda, K., Watanabe, I., Mizukami, K., Ban, S., and Takahashi, A.: Dry deposition of PM_{2.5} sulfate above a hilly forest using relaxed eddy accumulation, *Atmos. Environ.*, 107, 255-261, 10.1016/j.atmosenv.2015.02.050, 2015.
- Medlyn, B. E., Duursma, R. A., Eamus, D., Ellsworth, D. S., Prentice, I. C., Barton, C. V. M., Crous, K. Y., De Angelis, P., Freeman, M., and Wingate, L.: Reconciling the optimal and empirical approaches to modelling stomatal conductance, *Global Change Biology*, 17, 2134-2144, <https://doi.org/10.1111/j.1365-2486.2010.02375.x>, 2011.
- 585 Mendes, K. R. and Marengo, R. A.: Stomatal opening in response to the simultaneous increase in vapor pressure deficit and temperature over a 24-h period under constant light in a tropical rainforest of the central Amazon, *Theoretical and Experimental Plant Physiology*, 29, 187-194, 10.1007/s40626-017-0094-x, 2017.
- Mészáros, R., Horváth, L., Weidinger, T., Neftel, A., Nemitz, E., Dämmgen, U., Cellier, P., and Loubet, B.: Measurement and modelling ozone fluxes over a cut and fertilized grassland, *Biogeosciences*, 6, 1987-1999, 10.5194/bg-6-1987-2009, 2009.
- 590 Mills, G., Pleijel, H., Malley, C. S., Sinha, B., Cooper, O. R., Schultz, M. G., Neufeld, H. S., Simpson, D., Sharps, K., Feng, Z., Gerosa, G., Harmens, H., Kobayashi, K., Saxena, P., Paoletti, E., Sinha, V., and Xu, X.: Tropospheric Ozone Assessment Report: Present-day tropospheric ozone distribution and trends relevant to vegetation, *Elementa: Science of the Anthropocene*, 6, 10.1525/elementa.302, 2018.
- Mochizuki, T., Tani, A., Takahashi, Y., Saigusa, N., and Ueyama, M.: Long-term measurement of terpenoid flux above a Larix kaempferi forest using a relaxed eddy accumulation method, *Atmos. Environ.*, 83, 53-61, 10.1016/j.atmosenv.2013.10.054, 2014.



- 595 Monks, P. S., Archibald, A. T., Colette, A., Cooper, O., Coyle, M., Derwent, R., Fowler, D., Granier, C., Law, K. S., Mills, G. E.,
Stevenson, D. S., Tarasova, O., Thouret, V., von Schneidemesser, E., Sommariva, R., Wild, O., and Williams, M. L.: Tropospheric ozone
and its precursors from the urban to the global scale from air quality to short-lived climate forcer, *Atmos. Chem. Phys.*, 15, 8889-8973,
10.5194/acp-15-8889-2015, 2015.
- 600 Moravek, A., Foken, T., and Trebs, I.: Application of a GC-ECD for measurements of biosphere-atmosphere exchange fluxes of
peroxyacetyl nitrate using the relaxed eddy accumulation and gradient method, *Atmos. Meas. Tech.*, 7, 2097-2119, 10.5194/amt-7-2097-
2014, 2014.
- Muller, J. B. A., Coyle, M., Fowler, D., Gallagher, M. W., Nemitz, E. G., and Percival, C. J.: Comparison of ozone fluxes over grassland
by gradient and eddy covariance technique, *Atmospheric Science Letters*, 10, 164-169, <https://doi.org/10.1002/asl.226>, 2009.
- 605 Myneni, R., Knyazikhin, Y., and Park, T.: MCD15A3H MODIS/Terra+Aqua Leaf Area Index/FPAR 4-day L4 Global 500m SIN Grid
V006 [dataset], <https://doi.org/10.5067/MODIS/MCD15A3H.006>, 2015.
- Osterwalder, S., Fritsche, J., Alewell, C., Schmutz, M., Nilsson, M. B., Jocher, G., Sommar, J., Rinne, J., and Bishop, K.: A dual-inlet,
single detector relaxed eddy accumulation system for long-term measurement of mercury flux, *Atmos. Meas. Tech.*, 9, 509-524,
10.5194/amt-9-509-2016, 2016.
- Otu-Larbi, F., Conte, A., Fares, S., Wild, O., and Ashworth, K.: FORCAsT-gs: Importance of Stomatal Conductance Parameterization to
610 Estimated Ozone Deposition Velocity, 13, e2021MS002581, <https://doi.org/10.1029/2021MS002581>, 2021.
- Pattey, E., Desjardins, R. L., and Rochette, P.: Accuracy of the relaxed eddy-accumulation technique, evaluated using CO₂ flux
measurements, *Boundary-Layer Meteorology*, 66, 341-355, 10.1007/BF00712728, 1993.
- Piikki, K., De Temmerman, L., Ojanperä, K., Danielsson, H., and Pleijel, H.: The grain quality of spring wheat (*Triticum aestivum* L.) in
relation to elevated ozone uptake and carbon dioxide exposure, *European Journal of Agronomy*, 28, 245-254,
615 <https://doi.org/10.1016/j.eja.2007.07.004>, 2008.
- Popescu, F.: Transpiration and the economic coefficient of transpiration of Bezostaya wheat as dependent on soil moisture content, *Bul.*
stunt, Univ. Craiova., 9, 67-76, 1967.
- Ramírez, D. A., Yactayo, W., Rolando, J. L., and Quiroz, R.: Preliminary Evidence of Nocturnal Transpiration and Stomatal Conductance
in Potato and their Interaction with Drought and Yield, *American Journal of Potato Research*, 95, 139-143, 10.1007/s12230-017-9618-9,
620 2018.
- Rannik, Ü., Altimir, N., Mammarella, I., Bäck, J., Rinne, J., Ruuskanen, T. M., Hari, P., Vesala, T., and Kulmala, M.: Ozone deposition
into a boreal forest over a decade of observations: evaluating deposition partitioning and driving variables, *Atmos. Chem. Phys.*, 12,
12165-12182, 10.5194/acp-12-12165-2012, 2012.
- 625 Raupach, M. R. and Thom, A. S.: Turbulence in and above Plant Canopies, *Annual Review of Fluid Mechanics*, 13, 97-129,
10.1146/annurev.fl.13.010181.000525, 1981.
- Rawson, H. M. and Clarke, J. M.: Nocturnal transpiration in wheat, *Australian Journal of Plant Physiology*, 15, 397-406,
10.1071/pp9880397, 1988.
- Rawson, H. M., Begg, J. E., and Woodward, R. G.: The effect of atmospheric humidity on photosynthesis, transpiration and water use
efficiency of leaves of several plant species, *Planta*, 134, 5-10, 10.1007/BF00390086, 1977.
- 630 Reich, P. B., Sendall, K. M., Stefanski, A., Rich, R. L., Hobbie, S. E., and Montgomery, R. A.: Effects of climate warming on
photosynthesis in boreal tree species depend on soil moisture, *Nature*, 562, 263-267, 10.1038/s41586-018-0582-4, 2018.
- Ren, X., Sanders, J. E., Rajendran, A., Weber, R. J., Goldstein, A. H., Pusede, S. E., Browne, E. C., Min, K. E., and Cohen, R. C.: A
relaxed eddy accumulation system for measuring vertical fluxes of nitrous acid, *Atmos. Meas. Tech.*, 4, 2093-2103, 10.5194/amt-4-2093-
2011, 2011.
- 635 Schindlbacher, A., Zechmeister-Boltenstern, S., and Butterbach-Bahl, K.: Effects of soil moisture and temperature on NO, NO₂, and N₂O
emissions from European forest soils, *J. Geophys. Res. Atmos.*, 109, <https://doi.org/10.1029/2004JD004590>, 2004.
- Schoppach, R., Sinclair, T. R., and Sadok, W.: Sleep tight and wake-up early: nocturnal transpiration traits to increase wheat drought
tolerance in a Mediterranean environment, *Funct Plant Biol.*, 47, 1117-1127, 10.1071/fp20044, 2020.
- Seinfeld, J. H., Pandis, S. N., and Noone, K.: *Atmospheric Chemistry and Physics: From Air Pollution to Climate Change*, 2nd, John
640 Wiley & Sons, Inc., Hoboken, New Jersey, United States 2006.
- Stella, P., Loubet, B., de Berranger, C., Charrier, X., Ceschia, E., Gerosa, G., Finco, A., Lamaud, E., Serça, D., George, C., and Ciuraru, R.:
Soil ozone deposition: Dependence of soil resistance to soil texture, *Atmos. Environ.*, 199, 202-209, 10.1016/j.atmosenv.2018.11.036,
2019.
- Stella, P., Personne, E., Loubet, B., Lamaud, E., Ceschia, E., Béziat, P., Bonnefond, J. M., Irvine, M., Keravec, P., Mascher, N., and
645 Cellier, P.: Predicting and partitioning ozone fluxes to maize crops from sowing to harvest: the Surf_{atm}-O₃ model,
Biogeosciences, 8, 2869-2886, 10.5194/bg-8-2869-2011, 2011.
- Stella, P., Loubet, B., Laville, P., Lamaud, E., Cazaunau, M., Laufs, S., Bernard, F., Grosselein, B., Mascher, N., Kurtenbach, R., Mellouki,
A., Kleffmann, J., and Cellier, P.: Comparison of methods for the determination of NO-O₃-NO₂ fluxes and
chemical interactions over a bare soil, *Atmos. Meas. Tech.*, 5, 1241-1257, 10.5194/amt-5-1241-2012, 2012.



- 650 Stocker, D. W., Zeller, K. F., and Stedman, D. H.: O₃ and NO₂ fluxes over snow measured by eddy correlation, *Atmos. Environ.*, 29, 1299-1305, [https://doi.org/10.1016/1352-2310\(94\)00337-K](https://doi.org/10.1016/1352-2310(94)00337-K), 1995.
- Tai, A. P. K., Martin, M. V., and Heald, C. L.: Threat to future global food security from climate change and ozone air pollution, *Nature Climate Change*, 4, 817-821, 10.1038/nclimate2317, 2014.
- 655 Tamang, B. G., Schoppach, R., Monnens, D., Steffenson, B. J., Anderson, J. A., and Sadok, W.: Variability in temperature-independent transpiration responses to evaporative demand correlate with nighttime water use and its circadian control across diverse wheat populations, *Planta*, 250, 115-127, 10.1007/s00425-019-03151-0, 2019.
- Tang, G., Zhu, X., Xin, J., Hu, B., Song, T., Sun, Y., Zhang, J., Wang, L., Cheng, M., Chao, N., Kong, L., Li, X., and Wang, Y.: Modelling study of boundary-layer ozone over northern China - Part I: Ozone budget in summer, *Atmospheric Research*, 187, 128-137, <https://doi.org/10.1016/j.atmosres.2016.10.017>, 2017.
- 660 Tong, L., Xiao, H., Qian, F., Huang, Z., Feng, J., and Wang, X.: Daytime and Phenological Characteristics of O₃ and CO₂ Fluxes of Winter Wheat Canopy Under Short-Term O₃ Exposure, *Water, Air, & Soil Pollution*, 227, 4, 10.1007/s11270-015-2698-6, 2015.
- Tsai, J.-L., Tsuang, B.-J., Kuo, P.-H., Tu, C.-Y., Chen, C.-L., Hsueh, M.-T., Lee, C.-S., Yao, M.-H., and Hsueh, M.-L.: Evaluation of the relaxed eddy accumulation coefficient at various wetland ecosystems, *Atmos. Environ.*, 60, 336-347, 10.1016/j.atmosenv.2012.06.081, 2012.
- 665 van Meeningen, Y., Schurgers, G., Rinnan, R., and Holst, T.: Isoprenoid emission response to changing light conditions of English oak, European beech and Norway spruce, *Biogeosciences*, 14, 4045-4060, 10.5194/bg-14-4045-2017, 2017.
- Venables, W. N. and Ripley, B. D.: *Modern Applied Statistics with S*, Springer, New York, USA 2003.
- Vilà-Guerau De Arellano, J. and Duynkerke, P. G.: Influence of chemistry on the flux-gradient relationships for the NO-O₃-NO₂ system, *Boundary-Layer Meteorology*, 61, 375-387, 10.1007/BF00119098, 1992.
- 670 Wang, P., Yang, Y., Li, H., Chen, L., Dang, R., Xue, D., Li, B., Tang, J., Leung, L. R., and Liao, H.: North China Plain as a hot spot of ozone pollution exacerbated by extreme high temperatures, *Atmos. Chem. Phys.*, 22, 4705-4719, 10.5194/acp-22-4705-2022, 2022.
- Wang, T., Xue, L., Brimblecombe, P., Lam, Y. F., Li, L., and Zhang, L.: Ozone pollution in China: A review of concentrations, meteorological influences, chemical precursors, and effects, *Sci. Total Environ.*, 575, 1582-1596, <https://doi.org/10.1016/j.scitotenv.2016.10.081>, 2017.
- 675 Weber, B., Wu, D., Tamm, A., Ruckteschler, N., Rodríguez-Caballero, E., Steinkamp, J., Meusel, H., Elbert, W., Behrendt, T., Sörgel, M., Cheng, Y., Crutzen, P. J., Su, H., and Pöschl, U.: Biological soil crusts accelerate the nitrogen cycle through large NO and HONO emissions in drylands, *P. Natl. Acad. Sci.*, 112, 15384-15389, 10.1073/pnas.1515818112, 2015.
- Wild, O.: Modelling the global tropospheric ozone budget: exploring the variability in current models, *Atmos. Chem. Phys.*, 7, 2643-2660, 10.5194/acp-7-2643-2007, 2007.
- 680 Wu, X., Xu, Y., Shi, J., Zuo, Q., Zhang, T., Wang, L., Xue, X., and Ben-Gal, A.: Estimating stomatal conductance and evapotranspiration of winter wheat using a soil-plant water relations-based stress index, *Agricultural and Forest Meteorology*, 303, 108393, <https://doi.org/10.1016/j.agrformet.2021.108393>, 2021.
- Wu, Z. Y., Zhang, L., Wang, X. M., and Munger, J. W.: A modified micrometeorological gradient method for estimating O₃ dry depositions over a forest canopy, *Atmos. Chem. Phys.*, 15, 7487-7496, 10.5194/acp-15-7487-2015, 2015.
- 685 Xu, J., Zheng, Y., Mai, B., Zhao, H., Chu, Z., Huang, J., and Yuan, Y.: Simulating and partitioning ozone flux in winter wheat field: the Surf-atm-O₃ model (in Chinese), *China Environmental Science* 38, 455-470, 2018.
- Xu, M., Kasahara, K., Sorimachi, A., and Matsuda, K.: Nitric acid dry deposition associated with equilibrium shift of ammonium nitrate above a forest by long-term measurement using relaxed eddy accumulation, *Atmos. Environ.*, 256, 118454, <https://doi.org/10.1016/j.atmosenv.2021.118454>, 2021.
- 690 Xu, W., Kuang, Y., Zhao, C., Tao, J., Zhao, G., Bian, Y., Yang, W., Yu, Y., Shen, C., Liang, L., Zhang, G., Lin, W., and Xu, X.: NH₃-promoted hydrolysis of NO₂ induces explosive growth in HONO, *Atmos. Chem. Phys.*, 19, 10557-10570, 10.5194/acp-19-10557-2019, 2019.
- Xu, X.: Recent advances in studies of ozone pollution and impacts in China: A short review, *Current Opinion in Environmental Science & Health*, 19, 100225, <https://doi.org/10.1016/j.coesh.2020.100225>, 2021.
- 695 Xu, X., Bingemer, H. G., and Schmidt, U.: The flux of carbonyl sulfide and carbon disulfide between the atmosphere and a spruce forest, *Atmos. Chem. Phys.*, 2, 171-181, 2002.
- Xu, X., Lin, W., Xu, W., Jin, J., Wang, Y., Zhang, G., Zhang, X., Ma, Z., Dong, Y., Ma, Q., Yu, D., Li, Z., Wang, D., and Zhao, H.: Long-term changes of regional ozone in China: implications for human health and ecosystem impacts, *Elementa: Science of the Anthropocene*, 8, 10.1525/elementa.409, 2020.
- 700 Yang, W., Cao, J., Wu, Y., Kong, F., and Li, L.: Review on plant terpenoid emissions worldwide and in China, *Sci. Total Environ.*, 787, 147454, <https://doi.org/10.1016/j.scitotenv.2021.147454>, 2021.
- Yu, Q., Zhang, Y., Liu, Y., and Shi, P.: Simulation of the Stomatal Conductance of Winter Wheat in Response to Light, Temperature and CO₂ Changes, *Annals of Botany*, 93, 435-441, 10.1093/aob/mch023 %J Annals of Botany, 2004.
- Yuan, X., Calatayud, V., Gao, F., Fares, S., Paoletti, E., Tian, Y., and Feng, Z.: Interaction of drought and ozone exposure on isoprene emission from extensively cultivated poplar, *Plant, Cell & Environment*, 39, 2276-2287, <https://doi.org/10.1111/pce.12798>, 2016.
- 705



- Zhang, X., Xu, W., Zhang, G., Lin, W., Zhao, H., Ren, S., Zhou, G., Chen, J., and Xu, X.: Discrepancies in ozone levels and temporal variations between urban and rural North China Plain: Possible implications for agricultural impact assessment across China, *Elementa: Science of the Anthropocene*, 10, 10.1525/elementa.2022.00019, 2022a.
- 710 Zhang, X., Xu, W., Zhang, G., Lin, W., Zhao, H., Ren, S., Zhou, G., Chen, J., and Xu, X.: First long-term surface ozone variations at an agricultural site in the North China Plain: Evolution under changing meteorology and emissions, *Sci.Total Environ.*, 160520, <https://doi.org/10.1016/j.scitotenv.2022.160520>, 2022b.
- Zhu, Z., Sun, X., Zhao, F., and Meixner, F. X.: Ozone concentrations, flux and potential effect on yield during wheat growth in the Northwest-Shandong Plain of China, *Journal of Environmental Sciences*, 34, 1-9, <https://doi.org/10.1016/j.jes.2014.12.022>, 2015.
- 715 Zhu, Z., Sun, X., Dong, Y., Zhao, F., and Meixner, F. X.: Diurnal variation of ozone flux over corn field in Northwestern Shandong Plain of China, *Science China Earth Sciences*, 57, 503-511, 10.1007/s11430-013-4797-9, 2014.
- Zörner, J., Penning de Vries, M., Beirle, S., Sihler, H., Veres, P. R., Williams, J., and Wagner, T.: Multi-satellite sensor study on precipitation-induced emission pulses of NO_x from soils in semi-arid ecosystems, *Atmos. Chem. Phys.*, 16, 9457-9487, 10.5194/acp-16-9457-2016, 2016.